HHS Public Access

Author manuscript

Anal Chem. Author manuscript; available in PMC 2024 June 20.

Published in final edited form as:

Anal Chem. 2023 June 20; 95(24): 9227–9236. doi:10.1021/acs.analchem.3c00699.

Quantification of Irinotecan in Single Spheroids Using Internal Standards by MALDI Mass Spectrometry Imaging

Yijia Wang,

Department of Chemistry and Biochemistry, The Ohio State University, Columbus, Ohio 43210, United States

Amanda B. Hummon

Department of Chemistry and Biochemistry, The Ohio State University, Columbus, Ohio 43210, United States; Comprehensive Cancer Center, The Ohio State University, Columbus, Ohio 43210, United States

Abstract

Matrix-assisted laser desorption/ionization mass spectrometry imaging (MALDI-MSI) has been used to visualize molecular distributions in various biological samples. While it has succeeded in localizing molecules ranging from metabolites to peptides, quantitative MSI (qMSI) has remained challenging, especially in small biological samples like spheroids. Spheroids are a three-dimensional cellular model system that replicate the chemical microenvironments of tumors. This cellular model has played an important role in evaluating the penetration of drugs to better understand the efficacy of clinical chemotherapy. Therefore, we aim to optimize a method to quantify the distribution of therapeutics in a single spheroid using MALDI-MSI. Studies were performed with the therapeutic irinotecan (IR). The calibration curve showed a linear relationship with a limit of detection (LOD) of 0.058 ng/mm^2 and R^2 value at 0.9643. Spheroids treated with IR for different lengths of time were imaged using the optimized method to quantify the drug concentration during the penetration process. With a dosing concentration of 20.6 μM, the concentration of IR at 48 h of treatment was 16.90 μM within a single spheroid. Furthermore, spheroids were divided into different layers by spatial segmentation to be quantified separately. This MALDI-qMSI method is amenable to a wide range of drugs as well as their metabolites. The quantification results show great potential to extend this method to other small biological samples such as organoids for patient derived therapies.

Graphical Abstract:

Corresponding Author: Amanda B. Hummon – *Department of Chemistry and Biochemistry, The Ohio State University, Columbus, Ohio 43210, United States; Comprehensive Cancer Center, The Ohio State University, Columbus, Ohio 43210, United States;* Phone: 614-688-2580; hummon.1@osu.edu.

The authors declare no competing financial interest.

Complete contact information is available at: https://pubs.acs.org/10.1021/acs.analchem.3c00699

Supporting Information

The Supporting Information is available free of charge at https://pubs.acs.org/doi/10.1021/acs.analchem.3c00699.

Additional figures and tables showing MSI results normalized on TIC, results of heated tray comparison, measurement of single spheroid and layer sizes, detailed calculation equations and quantification results, relative response of decarboxylation IR (PDF)

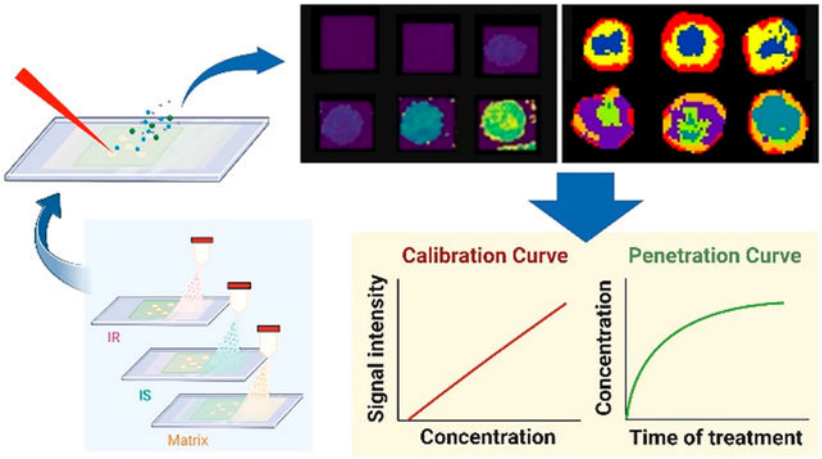

INTRODUCTION

Matrix-assisted laser desorption/ionization (MALDI) was first developed in the 1980s as a label-free, soft-ionization technology with great versatility in molecular coverage and compatibility with solid samples.[1] It was initially applied to mass spectrometry imaging (MSI) by Caprioli et al. to study the localization of peptides and proteins in different rat tissue sections.[2] Since then, MALDI-MSI has been widely used to study the distribution of various molecules including both endogenous[3] and exogenous[4] metabolites, lipids,[5] and drugs.[6] The ability of localize parent drugs and their metabolites simultaneously, combined with quantification strategies, has made MALDI-MSI an emerging tool in drug development and pharmaceutical research.[7]

Quantitative MSI (qMSI) using MALDI remains challenging because of the stability of analytes, inefficient analyte extraction, and ion suppression caused by matrix background signals, which especially impacts the quantification of small molecules in the low m/z range.[8,9] Furthermore, sample heterogeneity, mainly caused by matrix crystal dispersity and nonuniform cocrystallized substrate surfaces, can result in signal variations.[10] However, MALDI-MSI has unique advantages in quantification in that it has simplified sample preparation, high tolerance for salts, and much faster analysis speeds compared with the gold standard quantitative MS method, liquid chromatography tandem mass spectrometry (LC-MS/MS).[11] To capitalize on these advantages, many considerations need to be considered to conduct quantitative MALDI-MSI. These considerations include appropriate experimental design to optimize matrix selection and application, a normalization method to visualize data, and a suitable method used to generate calibration curves.[12]

Although difficult, quantification in various biological samples using MALDI-MSI has been successfully completed.[13,14] These studies include both relative quantification and absolute quantification. Relative quantification relies on an internal standard (IS) or an endogenous molecule in the sample to study the changes in concentrations, which are usually utilized in untargeted studies. For example, Ito and coauthors quantified amino acids and neurotransmitters using mTRAQ, an isotope label derivatization reagent, through a relative comparison of different slices of rat brain tissues.[13] In absolute quantification, the

concentrations of specific molecules are calculated directly, so it is mainly used in targeted studies. For example, Lan and coauthors established an absolute quantification method of 2-hydroxyglutarate using mouse liver as a mimetic model with ^{13}C labeled 2-HG disodium salt as an IS. This method was used on glioma tissues to identify isocitrate dehydrogenase mutant gliomas among 34 patients with 100% specificity and sensitivity.[14] However, most of the qMSI studies are based on large tissue samples with the size of several millimeters to centimeters.

Three-dimensional (3D) cell culture has emerged as a popular tool to bridge the gap between traditional monolayer cell culture and *in vivo* animal models.[15] Monolayer cell culture, which is also known as conventional two-dimensional cell culture, is used as a standard cell-based assay for testing drugs. In this model system, immortalized cells are grown either as an adherent monolayer on a substrate or in suspension.[16] This model is convenient and simple but fails to mimic the tumor microenvironment. Tissue samples based on animal models have more cellular and chemical complexity but, on the other hand, are more time-consuming and expensive. Thus, 3D cell cultures have become a popular model for obtaining a compromise between cost and complexity. These culture models are a powerful tool to evaluate novel therapeutics and offer the promise of improving preclinical selections.[17] Among all the 3D cell culture models, multicellular tumor spheroids play an important role, where one or more cell lines grow symmetrically to form cell aggregates that have complex cell–cell and cell–matrix interactions.[18] This symmetrical growth pattern produces the unique characteristics of spheroids, resulting in chemical gradients during growth, such as oxygen and nutrient gradients as well as the accumulation of waste products like lactate during metabolism (Figure 1A). These gradients make spheroids similar to avascular microregions in tumors so that they can closely mimic tumor microenvironments.[19] Cellular populations develop in the spheroids in response to the chemical gradients, with different layers including an outer proliferating region, a quiescent region, and a central necrotic core.[20]

It is important to expand qMSI beyond tissues to other biological samples like cell cultures. A recent report from the US Food and Drug Administration's Center for Drug Evaluation and Research (CDER) suggested the use of advanced alternatives to improve the predictivity of nonclinical drug testing as well as to potentially replace, reduce, or refine animal testing (3Rs).[21] These advanced technologies could improve the prediction of risk and the efficacy of toxicology thus helping to rapidly bring safer products to market. In the FDA's recommendations, various *in vitro* samples were declared as qualified alternative methods that incorporate the 3Rs, such as but not limited to organs-on-a-chip. For example, lung microphysiological systems were used to evaluate the toxicity induced by subacute exposures to formaldehyde fumes at different concentrations.[22] In another example, liver microphysiological systems were used to study drugs with high liver toxicity to demonstrate effectiveness and to suggest reduced risk.[23] All of these experiments have shown that advanced *in vitro* samples are critical to drug development and preclinical testing, while reducing the widespread dependence on animal models. Beyond organs-on-a-chip, other relevant techniques include 3D cell cultures like organoids and spheroids, which also follow the 3Rs as valuable potential replacements.[24]

Qualitative MALDI-MSI on spheroids was first demonstrated in 2011 by Li and Hummon with the mapping of several proteins in HCT 116 spheroids.[25] qMSI in spheroid samples remains challenging, though, because the limited sample size results in reduced sample extraction. There are several studies performing qMSI in spheroids based on different ionization strategies such as laser ablation coupled to inductively coupled plasma MSI (LAICP-MSI), which was used to quantify Pt- and Pd-based drugs in tumor spheroids.[26] This ionization method has superior spatial resolution but has limitations in that only metal-based molecules can be detected. Efforts have also been made to perform MALDI-qMSI in 3D cell culture models. For example, relative quantification was performed for irinotecan (IR) and its endogenous metabolites SN-38 and SN-38G to test the relative response against different concentrations of treatment in colorectal tumor organoids.[27] Another example of qMSI on single cell cultures was the quantification of IR on paper-based cell cultures (PBCs) with 2.85 mm diameter zones by Tobias and coauthors, though these paper-based cultures are larger than traditional 1 mm diameter spheroids. Calibration curves were generated in this study but were used to quantify Matrigel samples only with no biological samples.[28] While these studies have advanced applications of MALDI-qMSI for smaller 3D cell culture models, no results have yet been reported on individual spheroids.[29]

Therefore, the aim of this investigation is to obtain and optimize a MALDI-MSI method to quantify drug molecules as well as their metabolites in individual spheroids. These spheroids were grown for 14 days to a diameter of 1 mm, as the model system was originally defined by Robert Sutherland in 1971.[30] While some recent studies have grown spheroids for shorter amounts of time, we have determined that a 14-day growth period is necessary to develop the full complexity of the model system with the three representative cellular populations.[31,33] Furthermore, these mature spheroids can be divided into distinct layers by spatial segmentation to complete quantification of diverse molecules separately in different regions of each spheroid. As a proof-of-concept study, IR was chosen as a test therapeutic for initial studies, with d10-irinotecan used as the IS. The chemical structures of irinotecan and the deuterated form are shown in Figure 1B. IR has contributed to the treatment of solid tumors for more than 25 years. It triggers cell death by trapping the enzyme topoisomerase I on DNA and generating DNA breaks. Nowadays, it is also widely used in combination with other anticancer drugs.[41] Therefore, we chose IR to obtain absolute quantification through a time-dependent penetration process into individual HCT 116 spheroids.

In this study, two categories of spheroids were used: standard spheroids and dosed spheroids. Standard spheroids are control spheroids sprayed with IR and IS used to generate the calibration curves, while dosed spheroids are spheroids treated with IR during growth and are the targeted spheroids for quantification. Although IR is the only drug to be quantified in this proof-of-concept manuscript, the MALDI-qMSI method developed is amenable to a wide range of drugs as well as their metabolites and shows great potential to enable rigorous quantitative analysis of small biological samples such as individual spheroids and organoids for patient derived therapies.

EXPERIMENTAL SECTION

Chemicals and Reagents.

Irinotecan (IR) was purchased from Sigma-Aldrich (St. Louis, MO). D10-irinotecan was purchased from Clearsynth Laboratories (Canada) and was used as the internal standard (IS). 2,5-Dihydroxybenzoic acid (DHB) was purchased from Acros Organics (New Jersey)

Cell Culture and Spheroid Formation.

The colon carcinoma cell line HCT 116 was purchased from ATCC (Manassas, VA) and maintained in McCoy's 5A cell culture medium (Corning, Manassas, VA) with 10% fetal bovine serum (FBS) (VWR, Radnor, PA), 1% L-glutamine, and 1% penicillin–streptomycin (Life Technology, Grand Island, NY). Cells were grown at 5% CO_2 and 37 °C with media changes approximately every 4 days. Cell lines were used within 13 passages or two months after resuscitation of frozen aliquots from liquid nitrogen. The cell line was validated by short tandem repeat (STR) in 2022.

Spheroids were prepared following a standard protocol previously described.[25] HCT 116 cells were seeded into an agarose-based 96-well plate at a density of 7000 cells/well and incubated at 5% CO_2 and 37 °C. Beginning on Day 4, half volume media changes were completed every 48 h. Control spheroids were harvested on Day 14, while the drug treated spheroids were dosed with IR on Day 13 with a full volume media change at the final concentration of 20.6 μM and harvested for different times of treatment. This concentration was chosen based on our previous publication establishing the IC_{50} of IR in spheroids as 20.6 μM.[37]

Sample Preparation for MALDI Analysis.

Spheroids were washed in 1X phosphate buffered saline (PBS) (Gibco, Gaithersburg, MD) three times before being embedded in gelatin (Knox Unflavored Gelatin, CA) and were stored at −80 °C. The frozen pellets were cryosectioned using a Cryostat (Leica, Germany) into 12 μm thick slices and thaw-mounted onto indium tin oxide (ITO) coated glass slides (Delta Technologies Loveland, CO).

For the limit of detection (LOD) dried drop test, IR was dissolved in dimethyl sulfoxide (DMSO) (Invitrogen, Carlsbad, CA) at 100 mg/mL and diluted to different concentrations ranging from 0.1 μM to 100 μM in 50:50 (v/ v) ACN/H_2O. The solutions were hand-spotted in 0.5 μL volumes to each spheroid slice in triplicate and allowed to dry in the fume hood. A DHB solution was prepared at a final concentration of 10 mg/mL in 50:50 (v/v) ACN/H_2O with 0.1% trifluoroacetic acid (TFA) (EMB, Billerica, MA, USA). The matrix solution was filtered through a 0.22 μm filter and applied to the slides using a Model M5 TM-Sprayer (HTX Technologies, Chapel Hill, NC). The matrix was applied in eight passes in a crisscross pattern and using the following device settings: nozzle temperature, 75 °C; pressure, 10 psi; gas flow rate, 3 L/min; nozzle height, 40 mm; flow rate, 0.1 mL/min; moving velocity, 1000 mm/min; track spacing, 2 mm; dry time, 30 s.

For the calibration curve imaging experiments, IR solutions with different concentrations ranging from 3.13 μM to 50 μM were applied uniformly to the spheroid sections using the TM-sprayer two spray passes in a crisscross pattern with the following device settings: nozzle temperature, 30 °C; pressure, 10 psi; gas flow rate, 3 L/min; nozzle height, 40 mm; IS flow rate, 0.05 mL/min; moving velocity, 1000 mm/min; track spacing, 2 mm; dry time, 30 s. IR solutions were applied from low concentration to high concentration to different slides with a 10 min washing process in between using 50% methanol. After drying in the fume hood for an hour, the 100 μM IS solution was applied uniformly to the slides using the TM-sprayer with the same device settings as the IR spray passes. The slides were stored in the fume hood again for an hour to dry followed by DHB matrix spraying using the method described above. After matrix spraying, the slides were stored in the fume hood at room temperature for an hour and analyzed immediately afterward.

MALDI MSI Method and Data Acquisition.

All MALDI analyses including the dried drop test and MSI were performed on a Bruker SolariX 15T Fourier transform-ion cyclotron resonance (FTICR) mass spectrometer (Bruker Daltonics, Billerica, MA). Before analysis, the instrument was calibrated using red phosphorus by spotting in a region outside the sample with no gelatin or matrix. MALDI-MSI analysis was performed, and mass spectra were acquired in positive ion mode with 1000 laser shots per spot with 50 μm raster size and “small” as the laser focus. The sampling frequency was set to 2000 Hz. Mass spectra were acquired in a mass range of 300–1000 m/z. The general workflow is shown in Figure 2.

Dried drop test results were processed using DataAnalysis 4.4 while MSI data were processed using the SCILS Lab Pro 2022 software package to generate ion images with a semiquantitative color scale bar that was normalized to the total ion count of all the samples analyzed within the same file or normalized against the peak area of the IS. Quantification was performed in the SCiLS Lab software package under the quantitation method. Spatial segmentation was performed in the SCiLS Lab software package under the segmentation method, using a weak denoise and bisecting k-means clustering algorithm. The segmentation map was generated from a cluster dendrogram, which was further interrogated to discriminate regions to divide spheroids into different layers. Spheroid diameters and areas were measured using ImageJ 1.54d.

RESULTS AND DISCUSSIONS

Determining the LOD of MALDI-MSI Method.

To evaluate the spraying method from IR solutions and the LOD of IR on the spheroids, MSI experiments were completed by nebulizing IR solutions on the spheroid slides without addition of the IS. The MSI results were normalized against total ion count (TIC) of the average spectra for all the samples. IR was detected in all the samples with a concentration as low as 6.25 μM. IR was detected with an error between 1.0 to 1.3 ppm and MSI data was displayed at 587.285 $m/z \pm 2.4$ ppm mass window (Figure 3). The intensity box plot showed a notable difference between the 6.25 μM spheroids and control spheroids. With a two-tailed student t test, the two samples were significantly different with $t = 66.2628$ (p

< 0.0001) representing that the LOD of IR is lower than 6.25 μM. To test the LOD of the MSI method more quickly with fewer samples, dried drop tests were completed by pipetting IR standard solutions onto spheroid slices with lower concentrations followed by matrix spraying. The average scan of the instrument was set to one to better simulate an imaging method. Three spheroids were used for each concentration with three random positions tested in each spheroid. With a signal-to-noise ratio larger than 3, IR was detected at 587.286 *m*/*z* in all the conditions tested with the concentration as low as 0.78 μM. Considering that IR was not detected in all the three spheroids for low concentration conditions, 0.78 μM and 1.56 μM (Figure 3D), we conclude that the LOD of IR in spheroids is in the range of 1.56 μM to 3.12 μM.

Optimization of Spraying Methods.

In imaging studies, it is important to optimize the spraying method especially for the IS to minimize the analyte delocalization caused by the solvent to retain the spatial features.[32] Two methods established in previous studies were compared using the same sprayer settings with different solvents, aqueous[27] and ACN/H_2O 50:50 (v/v).[33] For the aqueous solvent, IR was detected at 587.286 *m*/*z* (1.5 ppm in error) and displayed at ±2.9 ppm mass window; the IS was detected at 597.349 *m*/*z* (1.4 ppm in error) and displayed at ±2.7 ppm mass window. For 50% ACN solvent, IR was detected at 587.286 *m*/*z* (0.2 ppm in error) and displayed at ±1.8 ppm mass window and the IS was detected at 597.349 *m*/*z* (0.2 ppm in error) and displayed at ±2.1 ppm mass window. Two normalization methods were used to analyze the imaging results, including total ion count (TIC) normalization of the average MS spectra and normalization against the peak area of the IS. When normalized against TIC, MSI results were compared with the samples without the IS to check if a different solvent for the IS would delocalize IR in the previous spraying (Figure S1). The data support that changing the solvent for spraying IS from 50% ACN to aqueous provided a completely different pattern of both IR and IS distribution in the images. The observed pattern is highly related to the difference in surface hydrophilicity. With 50% ACN used as solvent, IR concentrated on the spheroid regions while it migrated to the gelatin regions when using aqueous solvent. This delocalization is because the aqueous method requires a longer drying time. This longer time results in the IR redissolving and migrating to the more hydrophilic regions of the slides, which, in this case, are from the spheroid regions to the gelatin regions. Normalization against the peak area of the IS was used on spheroid regions of each imaging sample. These regions were manually selected based on a putative lipid at 782.56 *m*/*z* to compare the spraying method and determine which was more reproducible for quantification studies (Figure 4). From the results of the intensity box plots, signal intensities were more proportional to the IR concentrations when using 50% ACN solvent. Taking both of the factors described above into consideration, 50% ACN was determined to be the better solvent to spray IS compared with aqueous solvent and would be used in further studies.

Matrix deposition is an important requirement to ensure high-quality ion image detection in MALDI-MSI.[34] Previous studies established that matrix crystal size is inversely proportional to imaging spatial resolution.[35] To create smaller crystal sizes, many parameters need to be considered, including the flow rate of matrix solvent, moving velocity, and matrix

concentration.[44] The temperature of the tray is another critical factor to be optimized in the spraying process.[36] Two different matrices were sprayed at different tray temperatures with ambient temperature (25 °C) as the low temperature and 55 °C as the high temperature (Figure S2). IR was sprayed before the matrix at 50 μM. MSI results showed that a putative lipid was detected at 782.564 m/z ± 3.4 ppm that can be used to illustrate the region of spheroids, and IR was detected at 587.286 m/z ± 2.9 ppm. With similar imaging parameters, DHB works well to detect IR for imaging with great sensitivity. The intensity box plot showed a slight decrease in signal intensity of IR after increasing the tray temperature. The putative lipid showed slightly enhanced signal intensity after increasing the tray temperature using DHB and the very similar signal with α-cyano-4-hydroxycinnamic acid (CHCA) as the matrix. Considering these results, the data indicate that a higher tray temperature is beneficial to detecting some small endogenous species such as phosphatidylcholine, while ambient temperature is better for IR detection in the spheroids.

Calibration Curve and Quantification of IR in the Spheroids during Time-Dependent Penetration.

As a proof-of-concept study, we quantified IR in the spheroids during a time-dependent penetration process. IR was detected with an error of 0.2 ppm and the distribution was displayed in the mass window at 587.286 m/z ± 2.4 ppm. MSI data are displayed in Figure 5A. Three spheroids were imaged and analyzed as biological replicates for each condition. The images were normalized against the peak area of the IS, where the intensities of IS were set as 100%. The initial distribution patterns of IR and IS are shown in Figure S7 based on TIC normalization. To obtain absolute quantification, we need to convert the concentration of the spraying solutions into IR density based on the spraying method to generate a calibration curve (Table S1).[42] A calibration curve was linearly fitted to the dilution series of IR and analyzed together in SCiLS Lab with the IR dosed spheroids at different penetration times (Figure 5B). The calibration curves suggest a linear response over this concentration range with the LOD at 0.058 ng/mm^2, which corresponds to 1.97 μM IR standard solution, and R^2 value at 0.9643. Treated samples were prepared in two trials on different days with about a month in between. Trial 1 has only one time point at 24 h, and the samples were imaged in the same imaging run using the FT-ICR with the standard spheroids used to generate the calibration curve. Trial 2 has four different time points, 6, 24, 48, and 72 h, and these spheroids were prepared and imaged on different days using the same instrument and the same method settings. IR was not detected in the untreated control spheroids. For the dosed spheroids, IR localized predominantly in the outer region of the spheroids for the 6 h dosed spheroids and showed increasing signal intensity with a longer treatment time and fully penetrated the spheroids at the 24 h time point. This result is consistent with previously published imaging results.[37] To quantify IR uptake during the penetration, we calculated the concentration based on IR density with spheroid mass density, approximately 1000 fg/μm^3[43] (Table S2). Quantification results showed that, for Trial 2, concentrations of IR were 11.31 μM, 16.90 μM, and 21.26 μM for 6 h, 48 h, and 72 h treated spheroids, respectively. IR concentrations were calculated as 16.67 μM and 17.33 μM for the two trials for 24 h treated spheroids, separately. A penetration curve was generated in Figure 5C using concentration over time of treatment to show the IR concentration change during penetration. A two-tailed student t test was completed between the two trials for the

24-h treated spheroids. With a p-value = 0.5941 and t = 0.5783, by conventional criteria, this difference was not statistically significant with a 95% confidence interval. Compared to the calculated results, the quantification was reproducible once the calibration curve was generated.

Extended Applications of the Quantification Work-flow.

As described earlier in Figure 1A, cells were exposed to chemical gradients during the formation of the spheroids due to diffusion differences throughout the whole structure, forming several cellular layers within the spheroids including a proliferating region (outer layer), and a layer formed by quiescent and necrotic cells (inner layer).[38] The thickness of the layer is limited by the diffusion of oxygen, making the outer layer in the range of 150–200 μm.[20] Hence, spatial segmentation based on MS data for each pixel in the full mass range was completed within three replicates of each condition. This can divide spheroids into two regions to quantify IR separately in the different layers[40] (Figure 6A). For the standard spheroids, the inner regions were 603 μm in diameter on average. With spheroids 1050 μm in diameter on average, the inner region is about 57.3% thickness of the whole spheroid (Table S3). This value is consistent with previously published data.[20] For all the untreated control spheroids and the 6 h short time treated spheroids, the analyzed samples were segmented into three different regions. One of the segments represents the inner region, and the other two regions were combined together to represent the proliferating region. This region has a similar thickness to those in previous publications[38] with only one exception in the 12.5 μM standard samples. This sample has been removed as an outlier for further analysis. With the increase of IR treatment time, the cellular response to the drug made the microenvironment in the spheroid more complex, and more segmentation was required to divide the spheroids into two layers. Especially for the 72-h treated spheroids, five regions were segmented with two of them combined as the inner layer and three of them combined as the outer layer (Figure S4). This process has made it less precise and accurate to divide different layers based on spatial segmentation compared with the standard spheroids (Table S4). To solve this problem, we divided the two layers based on the thickness of the inner layer from the standard spheroids (Figure S5). Calibration curves were generated based on spatial segmentation of standard spheroids (Figure 6B), with a linear response over this concentration range with an LOD at 0.053 ng/mm^2 and R^2 value at 0.9618 for the inner layer and an LOD at 0.044 ng/mm^2 and R^2 value at 0.9838 for the outer layer. To reduce error caused by manually selecting different layers, we used the calibration curve for the inner layer to quantify IR concentration in the necrotic core and calculated IR concentration in the outer layer based on the results from the whole spheroid and the inner core (Table S5). The quantification results are shown in the penetration curve (Figure 6C). For Trial 2, concentrations of IR in the inner regions were 12.57 μM, 20.85 μM, 20.74 μM, and 22.91 μM for 6 h, 24 h, 48 h, and 72 h treated spheroids, respectively. The IR quantification results in the outer regions were 11.14 μM, 14.24 μM, 14.81 μM, and 20.40 μM for 6 h, 24 h, 48 h, and 72 h treated spheroids, respectively. The inner region and outer region had slightly different changes in IR concentration, with IR more concentrated in the inner region for a shorter time of treatment and distributing more homogeneously with a longer treatment time.

Multiple molecules could be quantified simultaneously, such as the metabolites of IR. Ions correlated to IR distribution were screened to find potential metabolites detected in the spheroids, and one exogenous metabolite of IR, the decarboxylation IR, was detected at 543.296 $m/z \pm 2.0$ ppm with a correlation value 0.774 ($p < 0.05$), which indicates significant colocalization of IR. Figure S3A shows that it has a very similar distribution in the standard spheroids but has much lower signal intensity in the IR dosed spheroids. However, decarboxylated IR cannot be purchased commercially to be added as a standard. To study the pattern and distribution change of decarboxylation IR during the penetration process, only a relative response to IR was calculated using the signal intensity of decarboxylation IR normalized against the peak area of the IS against IR concentration as the calibration curve. The interval on the x-axis was calculated to be 0.113 ng/mm^2, which is the limit of quantification (LOQ). When we tried to quantify the relative response in the dosed spheroids with different time points, the concentrations were as low as the LOQ, which means the method we use now is not sensitive to relatively quantify IR metabolites without a standard. However, it still shows the possibility to quantify several different molecules simultaneously during one experimental protocol.

CONCLUSIONS

In this study, we established a MALDI-qMSI method that is able to quantify therapeutics in small biological samples like single spheroids. As a proof-of-concept study, IR was chosen to perform the initial experiments. To optimize the qMSI method, the LOD of IR was determined using both dried drop and MSI methods on spheroid sections. The solvent used to spray the deuterium IS was optimized to reduce delocalization of the molecule of interest. The results showed that keeping the same solvent used for different spraying processes can better retain the original distribution of the molecules. A calibration curve was generated based on the optimized method with a linear relationship from 0.058 ng/mm^2 and R^2 value at 0.9643. Spheroids dosed during a time-dependent penetration process were used as targeted samples to quantify IR in a single spheroid region. With dosing at a concentration of 20.6 μM, at 48 h penetration time, IR was 16.90 μM within a single spheroid. We were able to divide spheroids into different layers using spatial segmentation to complete quantification within smaller regions to study the trend of concentration changes in each layer of a spheroid. Furthermore, by screening molecules correlated to IR, a decarboxylation metabolite of IR was found and relatively quantified to study its response to the drug.

While the methods developed in this study provide quantification of IR in individual spheroids only, they can easily be expanded for qMSI of other compounds, including a wide range of drugs, their metabolites, and endogenous molecules. Furthermore, it is the first time that MALDI-qMSI experiments have been completed on the scale of a single spheroid. With the sample size as small as 1 mm in diameter, the methods have the potential to quantify therapeutics in other small biological samples such as patient-derived organoids. The chemical properties for different molecules of interest will need to be evaluated to optimize the method to be specific for other drugs and small samples. These approaches will help with drug evaluation and personalized medicine development.

Supplementary Material

Refer to Web version on PubMed Central for supplementary material.

ACKNOWLEDGMENTS

Both Y.W. and A.B.H. are supported by NIGMS: R01 GM110406 and NIA: RF1AG072760. The 15 T Bruker SolariX FTICR instrument was supported by NIH Award Number Grant 1S10OD018507. The laboratory is also supported by P30 CA016058.

REFERENCES

(1). Hillenkamp F; Karas M Methods Enzymol. 1990, 193, 280–295. [PubMed: 1963669]

(2). Caprioli RM; Farmer TB; Gile J Anal. Chem. 1997, 69, 4751–4760. [PubMed: 9406525]

(3). Swales JG; Dexter A; Hamm G; Nilsson A; Strittmatter N; Michopoulos F; Hardy C; Morentin-Gutierrez P; Mellor M; andren PE; Clench MR Anal. Chem. 2018, 90 (10), 6051–6058. [PubMed: 29668267]

(4). Zecchi R; Franceschi P; Tigli L; Ricci F; Boscaro F; Pioselli B; Mileo V; Murgia X; Bianco F; Salomone F; Schmidt AF Respiratory research. 2019, 20 (1), 1–12. [PubMed: 30606211]

(5). Engel KM; Prabutzki P; Leopold J; Nimptsch A; Lemmnitzer K; Vos DN; Hopf C; Schiller J Prog. Lipid Res. 2022, 86, 101145. [PubMed: 34995672]

(6). Treu A; Kokesch-Himmelreich J; Walter K; Hölscher C; Römpp AJ Am. Soc. Mass Spectrom. 2020, 31 (11), 2277–2286.

(7). Castellino S; Groseclose MR; Wagner D Bioanalysis 2011, 3 (21), 2427–2441. [PubMed: 22074284]

(8). Chumbley CW; Reyzer ML; Allen JL; Marriner GA; Via LE; Barry III CE; Caprioli RM Anal. Chem. 2016, 88 (4), 2392–2398. [PubMed: 26814665]

(9). Duncan MW; Roder H; Hunsucker SW Brief funct genomics and proteomics 2008, 7 (5), 355–370.

(10). Rzagalinski I; Volmer DA Biochim Biophys Acta Proteins Proteom 2017, 1865 (7), 726–739. [PubMed: 28012871]

(11). Gachumi G; Purves RW; Hopf C; El-Aneed A Anal. Chem. 2020, 92 (13), 8628–8637. [PubMed: 32510944]

(12). Tobias F; Hummon AB J. Proteome Res. 2020, 19 (9), 3620–3630. [PubMed: 32786684]

(13). Ito T; Hiramoto M Anal Bioanal Chem. 2019, 411, 6847–6856. [PubMed: 31440782]

(14). Lan C; Li H; Wang L; Zhang J; Wang X; Zhang R; Yuan X; Wu T; Wu J; Lu M; Ma X Int. J. Cancer 2021, 149 (12), 2091–2098. [PubMed: 34224582]

(15). Lin RZ; Chang HY Biotechnol. J.: Healthcare Nutrition Technol. 2008, 3 (9–10), 1172–1184.

(16). Abbott A Nature. 2003, 424 (6951), 870–873. [PubMed: 12931155]

(17). Hirschhaeuser F; Menne H; Dittfeld C; West J; Mueller-Klieser W; Kunz-Schughart LA J. Biotechnol. 2010, 148 (1), 3–15. [PubMed: 20097238]

(18). Cui X; Hartanto Y; Zhang HJ R. Soc. Interface. 2017, 14 (127), 20160877. [PubMed: 28202590]

(19). Sutherland RM Science. 1988, 240, 177–184. [PubMed: 2451290]

(20). Alvarez-Pérez J; Ballesteros P; Cerdán S Magn. Reson. Mater. Phys. Biol. Med. 2005, 18, 293–301.

(21). Avila AM; Bebenek I; Bonzo JA; Bourcier T; Bruno KLD; Carlson DB; Dubinion J; Elayan I; Harrouk W; Lee SL; Mendrick DL Regul. Toxicol. Pharmacol. 2020, 114, 104662. [PubMed: 32325112]

(22). Ren B; Wu Q; Muskhelishvili L; Davis K; Wang Y; Rua D; Cao X Int. J. Mol. Sci. 2022, 23 (5), 2593. [PubMed: 35269734]

(23). Ribeiro AJ; Yang X; Patel V; Madabushi R; Strauss DG Clin. Pharmacol. Ther. 2019, 106 (1), 139–147. [PubMed: 30993668]

(24). Herrmann K; Pistollato F; Stephens ML ALTEX-Alternatives to animal experimentation. 2019, 36 (3), 343–352.

(25). Li H; Hummon AB Anal chem. 2011, 83 (22), 8794–8801. [PubMed: 21992577]

(26). Niehoff AC; Grünebaum J; Moosmann A; Mulac D; Söbbing J; Niehaus R; Buchholz R; Kröger S; Wiehe A; Wagner S; Sperling M Anal. Chim. Acta 2016, 938, 106–113. [PubMed: 27619092]

(27). Liu X; Flinders C; Mumenthaler SM; Hummon AB J. Am. Soc. Mass Spectrom. 2018, 29 (3), 516–526. [PubMed: 29209911]

(28). Tobias F; McIntosh JC; LaBonia GJ; Boyce MW; Lockett MR; Hummon AB Anal chem. 2019, 91 (24), 15370–15376. [PubMed: 31755703]

(29). Wang Y; Hummon AB J. Bio Chem. 2021, 297 (4), 101139. [PubMed: 34461098]

(30). Sutherland RM; McCredie JA; Inch WR J. Natl. Cancer Inst. 1971, 46 (1), 113–120. [PubMed: 5101993]

(31). Schroll MM; Liu X; Herzog SK; Skube SB; Hummon AB Nutr. Res. (N.Y.) 2016, 36 (10), 1068–1080.

(32). Huizing LR; Ellis SR; Beulen BW; Barré FP; Kwant PB; Vreeken RJ; Heeren RM Clin. Mass Spectrom. 2019, 12, 7–15. [PubMed: 34841074]

(33). Buck A; Halbritter S; Späth C; Feuchtinger A; Aichler M; Zitzelsberger H; Janssen KP; Walch A Anal Bioanal Chem. 2015, 407 (8), 2107–2116. [PubMed: 25311193]

(34). Veličković D; Zhang G; Bezbradica D; Bhattacharjee A; Paša-Tolić L; Sharma K; Alexandrov T; Anderton CR J. Am. Soc. Mass Spectrom. 2020, 31 (3), 508–516. [PubMed: 32126772]

(35). Trimpin S; Räder HJ; Müllen K Int. J. Mass Spectrom. 2006, 253 (1–2), 13–21.

(36). Technologies HTX, #41 Application Note - HTX Imaging: Effects of Tray Temperature on Matrix Deposition and Mass Spectrometry Imaging. 2018.

(37). Liu X; Weaver EM; Hummon AB Anal chem. 2013, 85(13), 6295–6302. [PubMed: 23724927]

(38). Chen Y; Wang T; Xie P; Song Y; Wang J; Cai Z Anal. Chim. Acta 2021, 1184, 339011. [PubMed: 34625248]

(39). Created with BioRender.com. 2022, https://app.biorender.com.

(40). Keithley RB; Weaver EM; Rosado AM; Metzinger MP; Hummon AB; Dovichi NJ Anal chem. 2013, 85 (19), 8910–8918. [PubMed: 24011091]

(41). Bailly C Pharmacol. Res. 2019, 148, 104398. [PubMed: 31415916]

(42). Technologies HTX, #31 Technical Note - Demonstration of matrix deposition optimization. Improving protein detection and reduction of analyte delocalization. 2015.

(43). Cristaldi DA; Sargenti A; Bonetti S; Musmeci F; Delprete C; Bacchi F; Pasqua S; Cavallo C; Bonsi L; Alviano F; Gazzola D Micromachines 2020, 11 (5), 465. [PubMed: 32354148]

(44). Gemperline E; Rawson S; Li L Anal chem 2014, 86 (20), 10030–10035. [PubMed: 25331774]

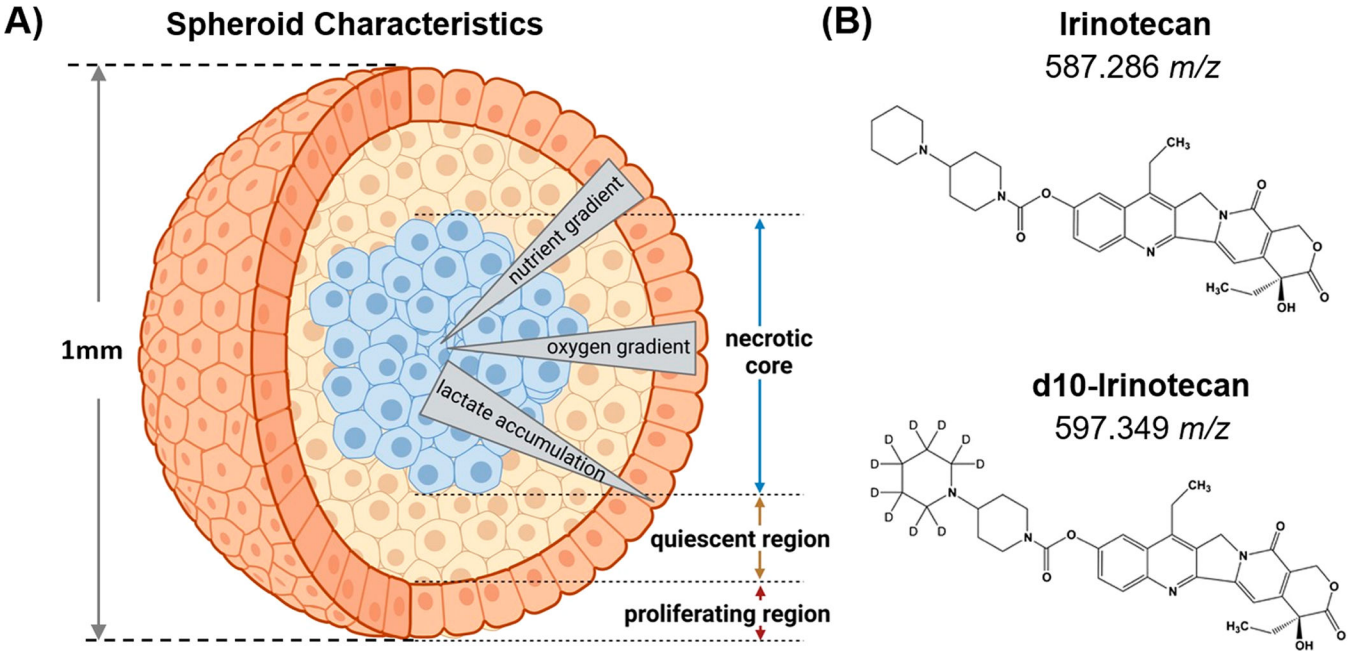

Figure 1.

Model of spheroids and structure of the model therapeutic IR: (A) spheroid characteristics; (B) chemical structure of IR and d10-IR as the internal standard.

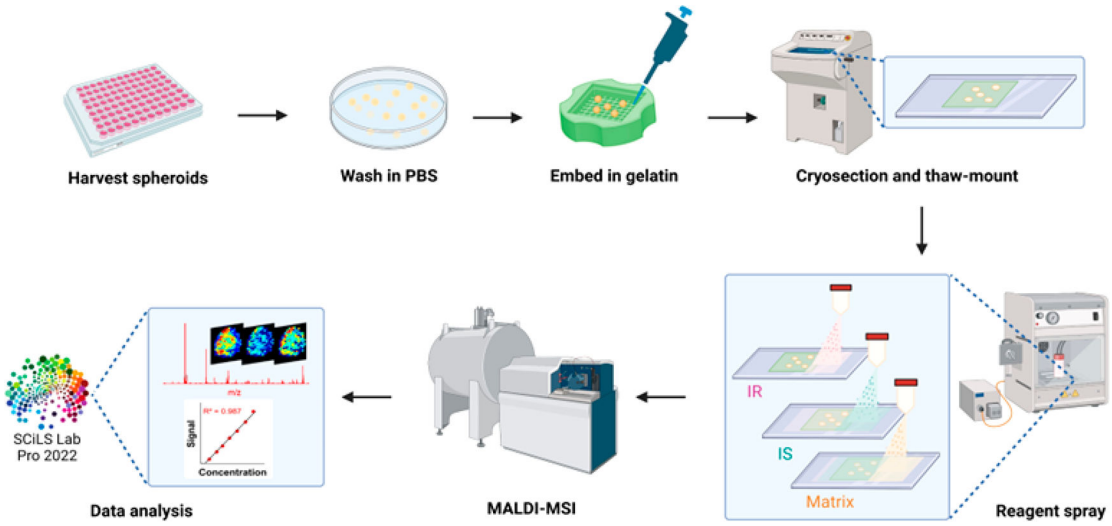

Figure 2.
Workflow of the quantification of IR using MALDI-MSI.[39]

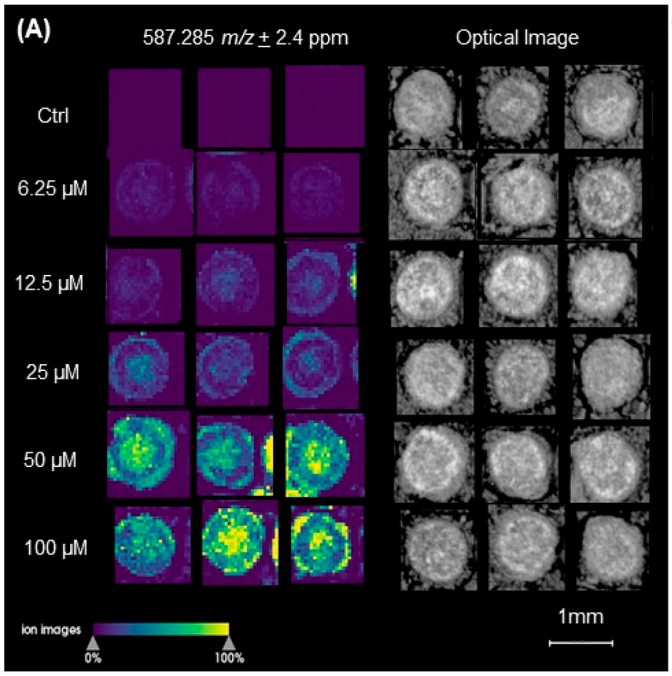

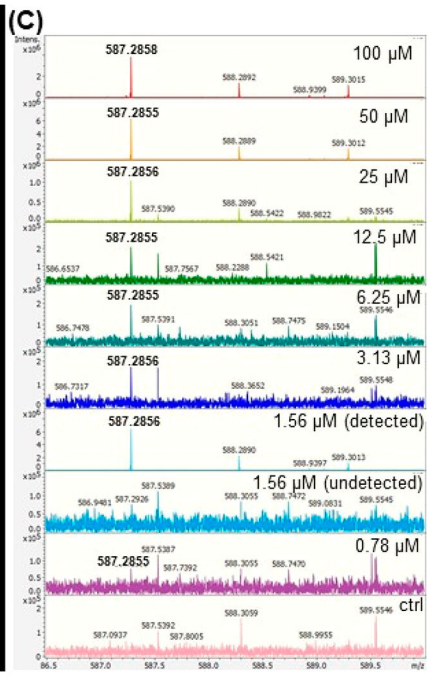

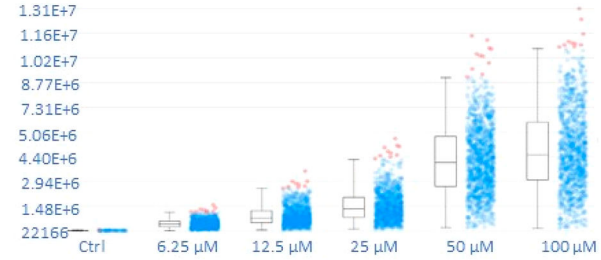

(D)

sample	#spectra detected	#spheroids detected	S/N
100 μM	9	3	490.0
50 μM	9	3	822.2
25 μM	9	3	132.5
12.5 μM	9	3	24.9
6.25 μM	8	3	22.5
3.12 μM	7	3	20.4
1.56 μM	3	1	826.8
0.78 μM	3	2	7.6
ctrl	0	0	------

Figure 3.

LOD study of IR in the spheroids without IS. (A) Optical image of spheroids analyzed and MSI of IR in the spheroids detected at 587.285 *m*/*z*. (B) Intensity box plot corresponds to MSI results showing that the signal intensity of IR kept increasing with the increase of IR concentration sprayed on the spheroids. With a two-tailed student *t* test, control samples and 6.25 *μ*M spheroids were significantly different ($p < 0.0001$). (C) Zoomed in dried drop test spectra of IR on the spheroid samples. IR was detected in all the concentrations except control samples. Three spheroids were used for each concentration with three random positions tested in each spheroid. Only one of the nine spectra for each condition is shown here as a representation. (D) Summary of dried drop tests which displayed number of spectra detected IR out of 9 spectra in total and number of spheroids detected IR out of 3 spheroids for each concentration. S/N for each concentration corresponds to samples in (C).

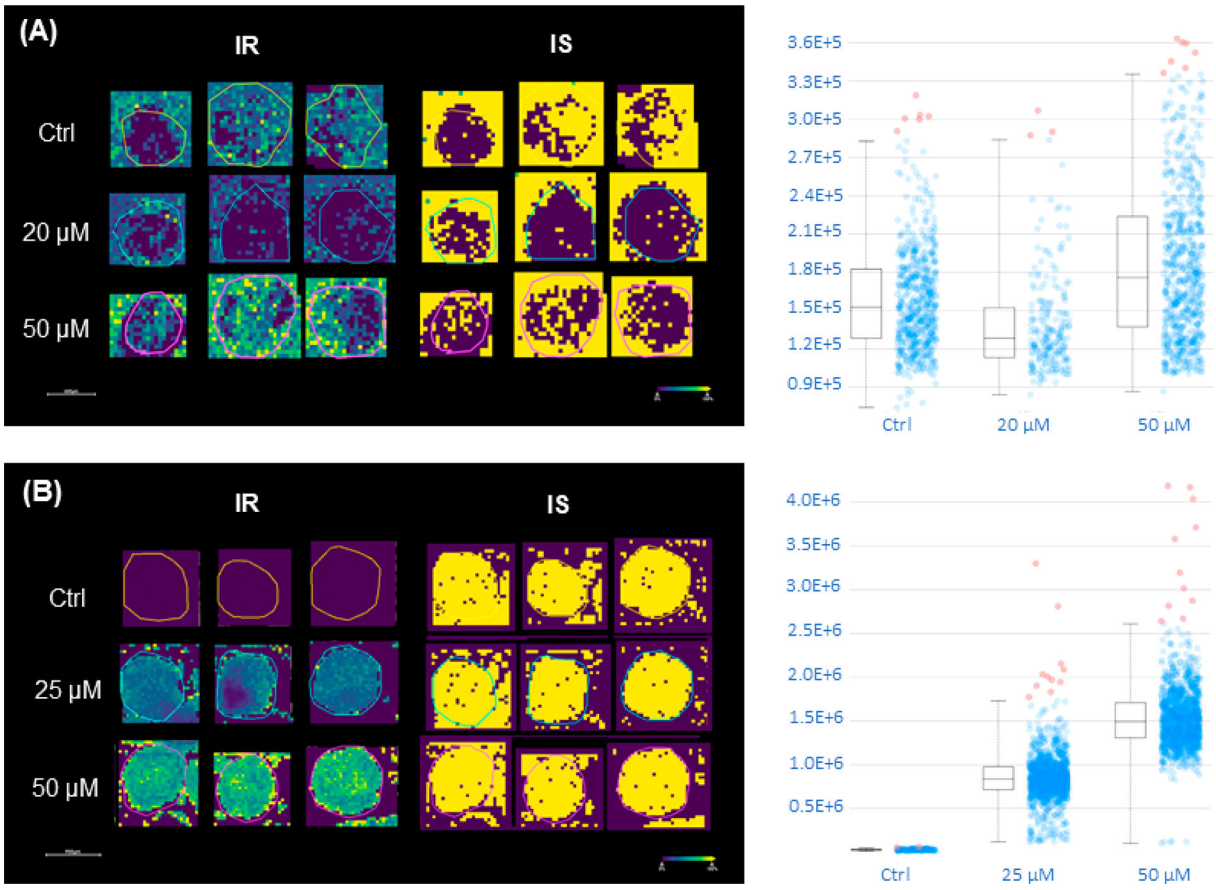

Figure 4.

MSI of IR to compare two solvents used to spray IS. (A) Aqueous solvent. Signal intensities of both IR and IS were higher outside of the spheroid regions. The intensity box plot showed that the signal intensities of IR are not proportional to the concentrations. (B) ACN/H2O 50:50 (v/v) as solvent. Signal intensities of IR and IS were higher in the spheroid regions. The intensity box plot showed that the signal intensities are proportional to the concentrations, and the average intensity was about ten times as those of aqueous solvent. Images were normalized against peak area of IS, which means that IS intensities were set as 100%.

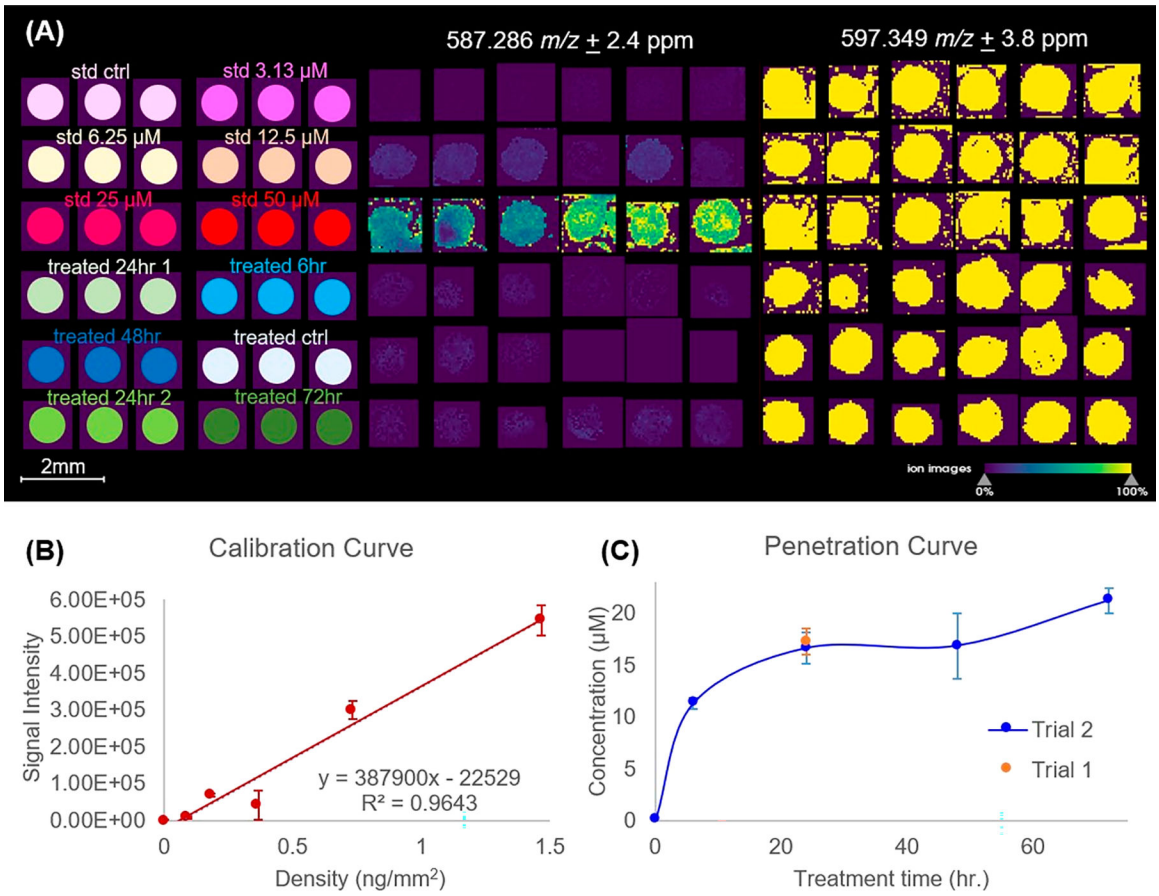

Figure 5.

qMSI of IR during penetration to spheroids. (A) MSI of IR and IS in the standard spheroids and dosed spheroids. IR was detected at 587.286 *m*/*z*, and IS was detected at 597.349 *m*/*z*. Data normalized against peak area of IS. (B) Calibration curve of IR quantification. The error bar shown is based on the quantified results of three spheroids. (C) Penetration curve showing the IR concentration changes in the whole spheroids with the increase of time of treatment.

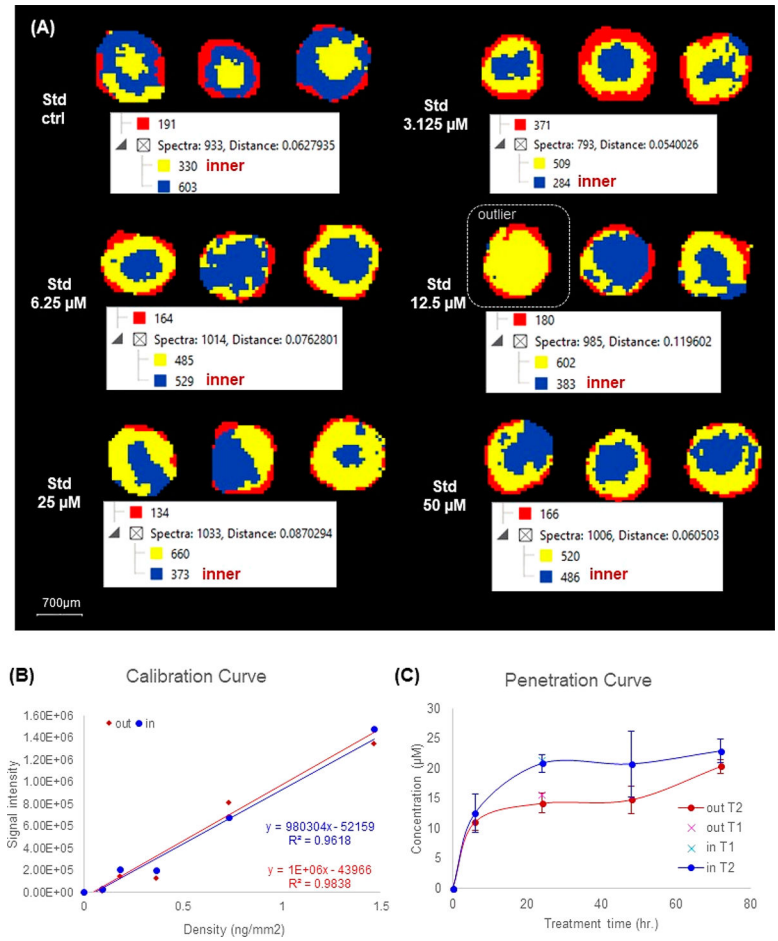

Figure 6.

qMSI of IR in the inner and outer layer of spheroids. (A) Spatial segmentation of standard spheroids divided each spheroid into inner and outer layers. (B) Calibration curve of IR quantification for inner and outer region separately. (C) Penetration curve showing the IR concentration changes in the inner or outer region of spheroids with the increase of time of treatment. The error bar shown is based on the quantified results of three spheroids.